An Experimental Study on Permeability of Kimachi Sandstone in Deformation and Failure Process under Deviator stress

Michihiko Takada and Yoshiaki Fujii
[1]Graduate School of Engineering, Hokkaido University, Sapporo, Japan

Abstract: Permeability of Kimachi sandstone in deformation and failure process was investigated. Tests were carried out under a constant confining pressure of 5.0, 7.5, or 10.0 MPa with a pore pressure of 2.0 MPa. Cylindrical test specimens with a diameter of 30.0 mm and a length of 60.0 mm were used. 0.2% of axial compressive strain was applied at a time and a permeability test by the transient-pulse method was carried out at each step after 3 hour delay time to settle down deformation. This step was repeated until axial strain reached about 5.0%. The stress-strain relation was linear in low deviator stress and gradually became nonlinear as peak strength approached. The permeability decreased in the elastic region and then increased as the peak strength approached. In residual strength region, the permeability also increased at first, but it decreased after then.

Keywords: permeability, sedimentary rock, fracture, deviator stress.

1. Introduction

Water advection is one of the main mechanisms of subsurface mass transportation. Prediction of mass transportation is required in a variety of areas, for example, geological disposal, remediation of ground pollution, geothermal power generation, petroleum reservoir development etc. In this respect, knowledge on rock permeability in various conditions is important. Sometimes surrounding rock of an underground structure is damaged by excavation. This damaged zone is called EDZ, short for excavation damage or disturbed zone. Research on permeability of damaged rock is needed to accurately estimate mass transport around an underground structure. Moreover, rock permeability is closely related to its internal structure, so it is useful if relation between permeability and damage of rock is clarified.

Internal structure of rock rapidly changes in failure process. Under deviator stress, at first rock deforms relatively elastically but as deviator stress increases, damage in rock gradually progresses. It is considered that numerous microcracks are generated and grow in the vicinity of peak strength. Those microcracks form macroscopic faults at failure and rock reaches residual strength. In residual strength region, deviator stress does not vary much but rock structure remains to change significantly. Permeability also changes in this process. The purpose of this study is to clarify how and why permeability changes in failure process.

Ngwenya et al. [1] has studied on permeability change of Clashach sandstone in failure process. Clashach sandstone has permeability in a range of 10^{-13} to 10^{-12} m^2 and porosity of about 20% (1 $m^2 \approx 10^{12}$ darcy). The permeability of Clashach sandstone is about 6 orders larger than that of Kimachi sandstone. In their experiments, permeability of Clashach sandstone was slightly increased at failure and gradually decreased with increased axial strain after failure. They considered that the permeability decrease after failure is linked to the microstructural change of flow path which occurred by the cataclastic fault sealing. They used the flow pump method and the steady state solution to calculate permeability. However this method might not be applicable to low permeable rocks since it takes a long time to reach a steady state for such rocks.

Westerly granite in failure process was also studied by Kiyama et al. [2]. Their experiments were carried out under constant confining pressures of 10 to 75 MPa and a constant lateral strain rate. Permeability was measured by the transient pulse method (Brace et al. [3]) and was about 10^{-19} m^2 under hydrostatic pressure of 10 MPa. The permeability was slightly decreased at low deviator stress and increased as peak strength approached. After failure, the permeability increased approximately 10^2 times. Under high confining pressures, change in permeability was small.

1.1. Permeability model

Some permeability models that connect permeability and other physical properties have introduced in past studies. These models are useful to estimate permeability from other physical properties and to consider internal structure of rock from measured permeability. These models are based on either Hagen-Poiseuille equation that describes slow viscous incompressible flow through a constant circular cross section or Couette-Poiseuille equation that describes slow viscous incompressible flow through a constant width flat plate.

Kozeny-Carman model

According to Wyllie et al. [4], Kozeny-Carman model was introduced by Kozeny et al. [5] and developed by Carman [6]. This model is based on the assumptions that pores can be modeled as channels whose shape is the same with each other, and that total surface area and volume of these channels are equal to those of pores. This model was proposed for unconsolidated particle aggregate but it is believed to be applicable to some type of

such rocks as sandstones. Kozeny-Carman equation is written as

$$\frac{q}{A} = \frac{1}{k_0}\left(\frac{L}{L_e}\right)^2 \frac{\eta^3}{S_v^{\,2}(1-\eta)^2}\frac{\Delta p}{\mu L}, \quad (1)$$

where q is flow rate of fluid, A is bulk cross-sectional area, η is porosity, S_v is volumetric basis specific surface area, Δp is fluid pressure difference between upstream and downstream, μ is viscosity of pore fluid, L is geometrical length of a medium in the direction of macroscopic flow, L_e / L is tortuosity and k_0 is the shape factor. k_0 has a range of about 2.0 to 3.0 and is equal to 2.0 in case of a circular channel and 3.0 in case of a flat plate channel. Tortuosity is the ratio of effective length of fluid flow in the porous medium to L. In this model, mean hydraulic radius m has the relation shown below.

$$m = \frac{\eta}{S_v}. \quad (2)$$

For a small porosity, equation (1) is rewritten as

$$\frac{q}{A} = \frac{m^2}{k_0}\left(\frac{L}{L_e}\right)^2 \eta \frac{\Delta p}{\mu L}. \quad (3)$$

This form is the same as Brace et al. [3].

According to Garrouch et al. [7], tortuosity can be evaluated from electrical resistivity or molecular diffusivity. Some electrical resistivity models and molecular diffusivity models for tortuosity was referred by Garrouch et al. [7]. These models have forms of

$$\frac{L_e}{L} = \left(\eta \frac{R_{\text{fluid}}}{R_{\text{bulk}}}\right)^n, \text{ or} \quad (4)$$

$$\frac{L_e}{L} = \left(\eta \frac{D_{\text{bulk}}}{D_{\text{fluid}}}\right)^n, \quad (5)$$

where R_{fluid} is electric resistance of fluid, R_{bulk} is that of porous medium filled with fluid, D_{fluid} is molecular diffusion coefficient in fluid, D_{bulk} is effective diffusion coefficient of porous medium and n is a constant in the range between 0.5 and 2.0.

1.2. Physical properties of Kimachi sandstone

Kimachi sandstone has been studied in the field of rock mechanics in Japan and some physical properties are known. **Table 1** shows true density, effective porosity, permeability, tortuosity and specific surface area of Kimachi sandstone that were measured in the past researches and this study. Data roughly coincide with each other except for permeability, which show a wide variation. One of the reasons of the wide variation may be due to the difference of measurement methods or experimental apparatus.

2. Experimental methods

2.1. Test specimens

The experiments were carried out on specimens of Kimachi sandstone quarried from Shimane Prefecture, Japan. Specimens were drilled to a diameter of 30 mm from a block then they were cut to a length of 60 mm. End faces of specimens were ground to a flatness of ±0.02 mm. Two cross type strain gages were glued on the sides of each specimen by gelled alpha-cyanoacrylate adhesive to measure strain. End faces of specimens were directly attached to stainless steel end pieces. The end pieces have a center hole for water supply. Side of each specimen was coated with silicon rubber. Then the connected end pieces and specimens were covered with a heat shrinkable tubing and saturated with pure water.

2.2. Experimental Apparatus

Ultra compact triaxial vessel developed by Fujii [14] was used for triaxial loading. **Figure 1** shows a schematic figure of experimental apparatus. Axial stress was controlled by a loading frame and confining pressure was applied by a water pump. Pore fluid pressure was controlled by a syringe pump and supplied through the end pieces.

2.3. The transient pulse method

The transient pulse method, which was introduced first by Brace et al. [3], was utilized to measure permeability in this study. This method is applicable to low permeability rock, and can be conducted within a relatively short time. Permeability can be calculated by the approximate solution by Brace et al. [3] or the exact analytical solution by Hsieh et al. [15]. With use of the exact solution, not only permeability but also specific storage coefficient of a

Table 1. Some physical properties of Kimachi sandstone:

References	True density, ρ_p (kg/m^3)	Effective porosity, η	Permeability, k (m^2)	Tortuosity, L_e/L	Specific surface area, S_w (m^2/kg)
Hirono et al. [8]	2701	0.230		5.1	
Takahashi et al. [9]			$1.98*10^{-17}$		
Nakamura et al. [10]	2546	0.2223	$4.41*10^{-18}$		$5.75*10^{-3}$
Lin et al. [11]		0.19			$5.0*10^{-3}$
Sugimoto et al. [12]		0.254	$1.60*10^{-18}$		
Kumakura et al. [13]			$3.07*10^{-18}$		
This study			$2.16*10^{-18}$		

specimen can be calculated. However the exact solution is complicated, so the approximate solution still has usability. We used the approximate solution to calculate permeability.

Figure 2 schematically shows experimental apparatus of the transient pulse method. There are a reservoir at each end of a test specimen. Permeability was measured through the following steps. First, reservoirs and a specimen were subjected to a equal pore pressure p_0. Here we call water pressure of upstream reservoir p_1 and that of downstream reservoir p_2. Then p_1 was slightly raised. **Figure 3** shows relation between fluid pressure and time.

The approximate solution is

$$\frac{\mathrm{d}[\ln(p_1 - p_2)]}{\mathrm{d}t} = -A\frac{k}{\mu L}\frac{S_1 + S_2}{S_1 S_2}, \qquad (6)$$

where k is permeability, S_1 and S_2 are compressive storage of upstream and downstream reservoir, respectively.

2.4 Experimental steps of the permeability test

Permeability experiments were conducted as the following steps.

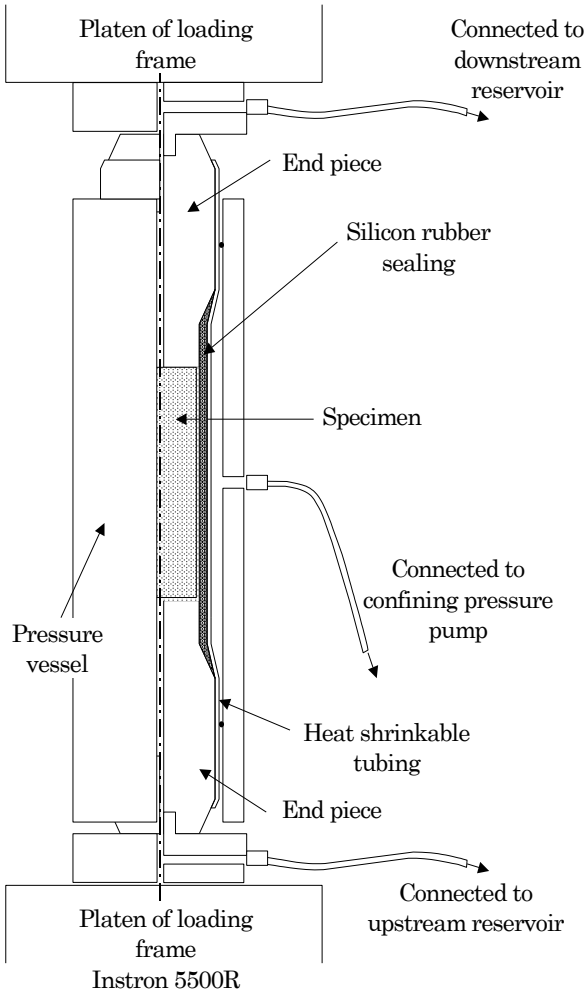

Figure 1. Experimental apparatus.

step1: Hydrostatic fluid pressure equal to a confining pressure was applied to a specimen. Applied confining pressure was 5.0, 7.5 or 10.0 MPa and pore pressure was 2.0 MPa. Then, approximately 3 hours of delay time was given to settle down deformation and pore pressure.

step2: A permeability test by transient pulse method was conducted. It took about 20 to 60 minutes for one test. Pulse increase of upstream pressure was approximately 0.2 MPa.

step3: 0.2% of axial compressive strain was applied. Then, approximately 3 hours of delay time was given to settle down deformation and pore pressure.

step4: **step2** and **step3** were repeated until axial strain reached approximately 5.0% at approximately 5 hour interval. Permeability tests were conducted only in daytime.

2.5. Pore deformation measurement

Pore deformation of Kimachi sandstone was measured by the syringe pump during triaxial compression tests. Tests were conducted under condition of constant confining pressures of 5.0 or 10.0 MPa and a constant axial strain rate of 0.012, 0.036 or 0.0036 mm/min. The pump has a capability to measure volume change with a resolution of

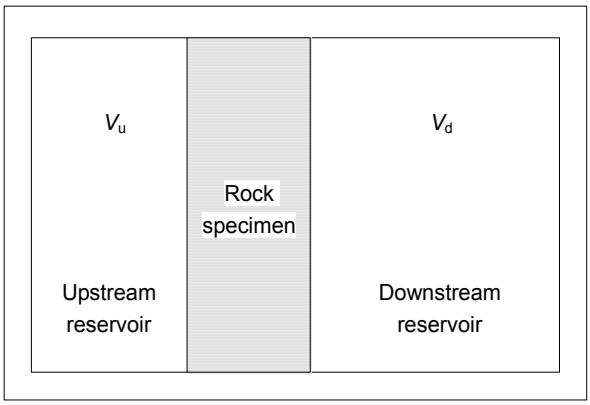

Figure 2. Schematic figure of experimental apparatus for the transient pulse method.

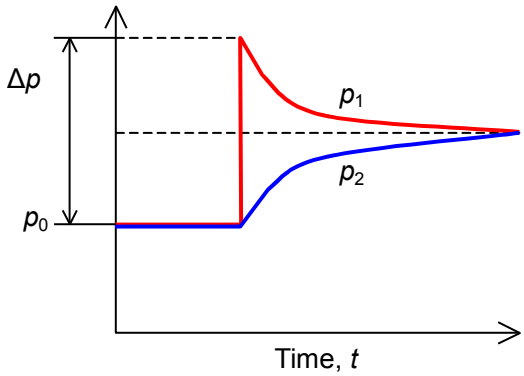

Figure 3. Decay of differential pressure between upstream and downstream reservoirs in the transient pulse method.

10^{-12} m^3. Deformation of specimens was also measured by strain gauges.

3. Experimental results

3.1. Deformation behavior

Figure 4 shows stress-strain relation measured by strain gauges. The stress-strain relation was relatively linear in low deviator stress region and gradually changed to nonlinear as peak deviator stress approached. Lower graph of **Figure 5** shows relation between deviator stress and axial strain calculated from the platen stroke. As this graph shows, specimens reached peak strength at about 1% of axial strain, and reached residual strength at 3 to 4% of axial strain.

The point of macroscopic failure is not clear but it would be near the residual strength, since the specimen experienced 2% axial strain did not have an apparent macroscopic rapture plane but specimen experienced 3% axial strain had it in the observation of specimens after experiments.

Figure 6 shows a photograph of specimens after tests. Three specimens from left to right in this photograph were used in each experiment conducted under a confining pressure of 5.0, 7.5 or 10.0 MPa. All three specimens had a macroscopic rapture plane but that of the specimen under 5.0 MPa confining pressure was more apparent than the others.

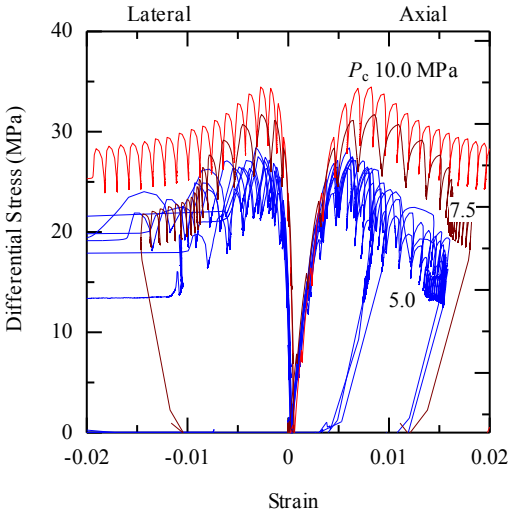

Figure 4. Stress-strain relation measured by strain gauges.

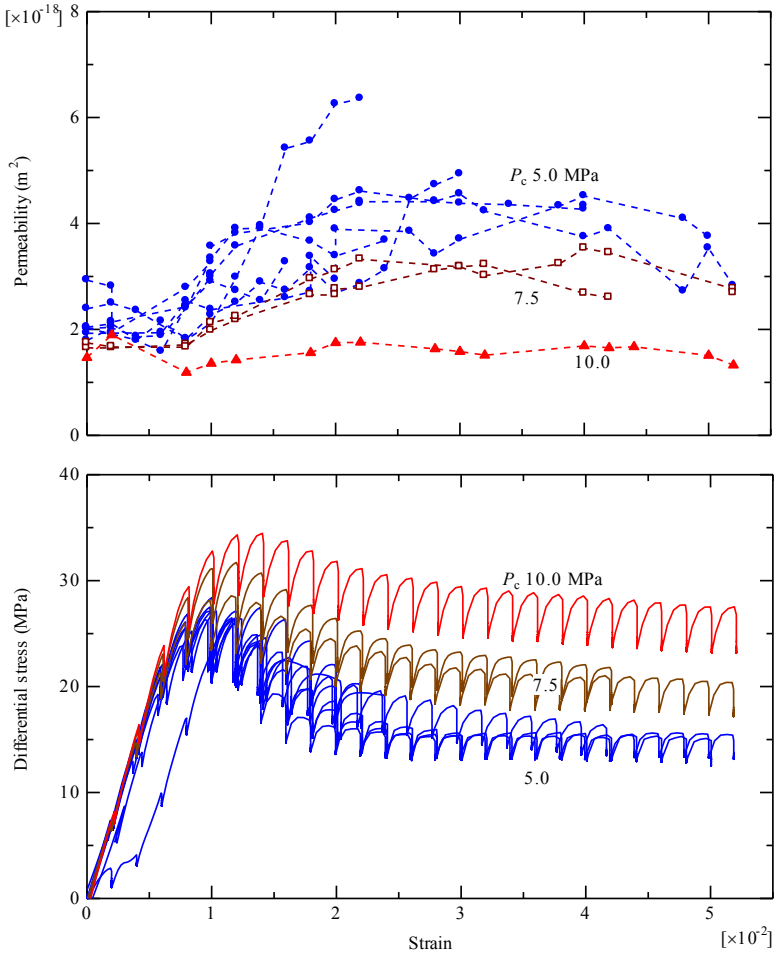

Figure 5. Upper graph: relation of permeability and axial strain calculated from stroke of the platen. Lower graph: relation of differential stress and axial strain calculated from platen stroke.

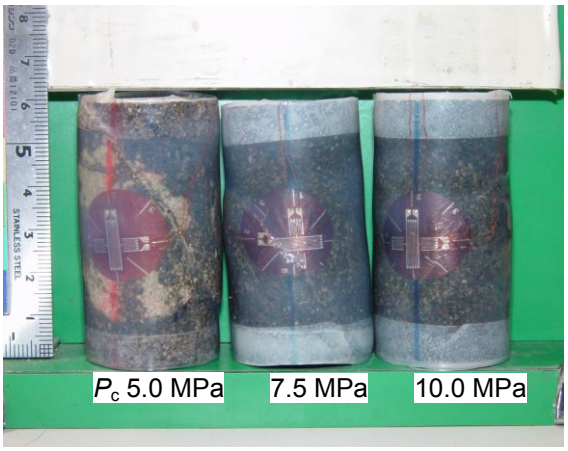

Figure 6. Specimens after test.

3.2. Cohesion and internal friction angle

Cohesion and internal friction angle of Kimachi sandstone in Mohr-Coulomb criterion were calculated as shown in **Table 2**. **Figure 7** shows the relation between effective strength and effective confining pressure.

Table 2. Cohesion and Internal friction angle.

	Cohesion (MPa)	Internal friction angle (degree)
Peak strength	12.27	24.8
Residual strength (from origin)	0.0	40.6
Residual strength	4.33	30.5

3.3. Permeability change

Upper graph of **Figure 5** shows relation between permeability and axial strain calculated from platen stroke. The permeability slightly decreased at first and it began to increase in the vicinity of peak strength. In residual strength region, the permeability also increased at first and gradually decreased as axial strain increased. The effect of confining pressure was clear. In the experiment under 10.0 MPa confining pressure, the permeability change was relatively small and in cases of 5.0 MPa confining pressure, the permeability changed significantly after failure.

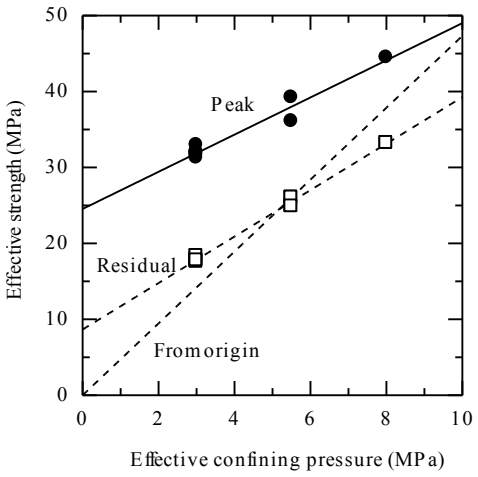

Figure 7. Relation between effective strength and Effective confining pressure.

3.3 Results of pore deformation measurement

Figure 8 shows relation of deviator stress and volumetric strain which was measured by the syringe pump and strain gauges. Volumetric strain, which was measured by the syringe pump, is the ratio of volume change of pore fluid to initial bulk specimen volume. It does not include strain of solid part of the specimen. Volumetric strain measured by strain gauges, is regarded as entire strain of a specimen. Volumetric strain measured by syringe pump should be smaller than by strain gauges but this was not always true in the results. Volumetric strain measured by syringe pump was close to that by strain gauges when stroke speed was low and confining pressure was high.

4. Discussion

4.1. Permeability change in deformation and failure process

The results of pore deformation measurement tests show that entire deformation of a specimen was close to that of pore deformation. This means that deformation of solid part was relatively small and porosity can be written as

$$\eta \cong \eta_0 - \varepsilon_V . \tag{7}$$

where η_0 is porosity at atmospheric pressure and ε_V is compressive volumetric strain, although this might not be true for other kind of rocks. Porosity change during the experiments was smaller than 1% and too small to induce measured change in permeability. Therefore microscopic structure change would be the main reason of the change in permeability.

Permeability decrease in linear elastic region would have occurred by closure of flow path. At high deviator stress, the stress-strain relation was non linear and the stiffness in the axial direction decreased. This deformation behavior would be induced by the structural change of rock matrix. It is considered that mineral particles behave as a linear elastic material at such low stress as several ten MPa. Mean stress of specimen can be described as

$$\begin{aligned} \langle \sigma_{ij} \rangle &= \frac{1}{V}\left(\int_{V^{\mathrm{Solid}}} \sigma_{ij} \mathrm{d}V + \delta_{ij} \int_{V^{\mathrm{Pore}}} P^{\mathrm{Pore}} \mathrm{d}V \right), \\ &= (1-\eta)\left\langle \sigma^{\mathrm{Solid}}{}_{ij} \right\rangle + \delta_{ij} \eta P^{\mathrm{Pore}} \end{aligned} \tag{8}$$

where ‹σ_{ij}› is mean stress of a specimen, V is bulk volume of a specimen, V^{Solid} is volume of solid part of a specimen, V^{Pore} is volume of pore of a specimen and P^{Pore} is pore fluid pressure. The decrease of stiffness in axial direction would be induced by some partial rotational deformation. This deformation

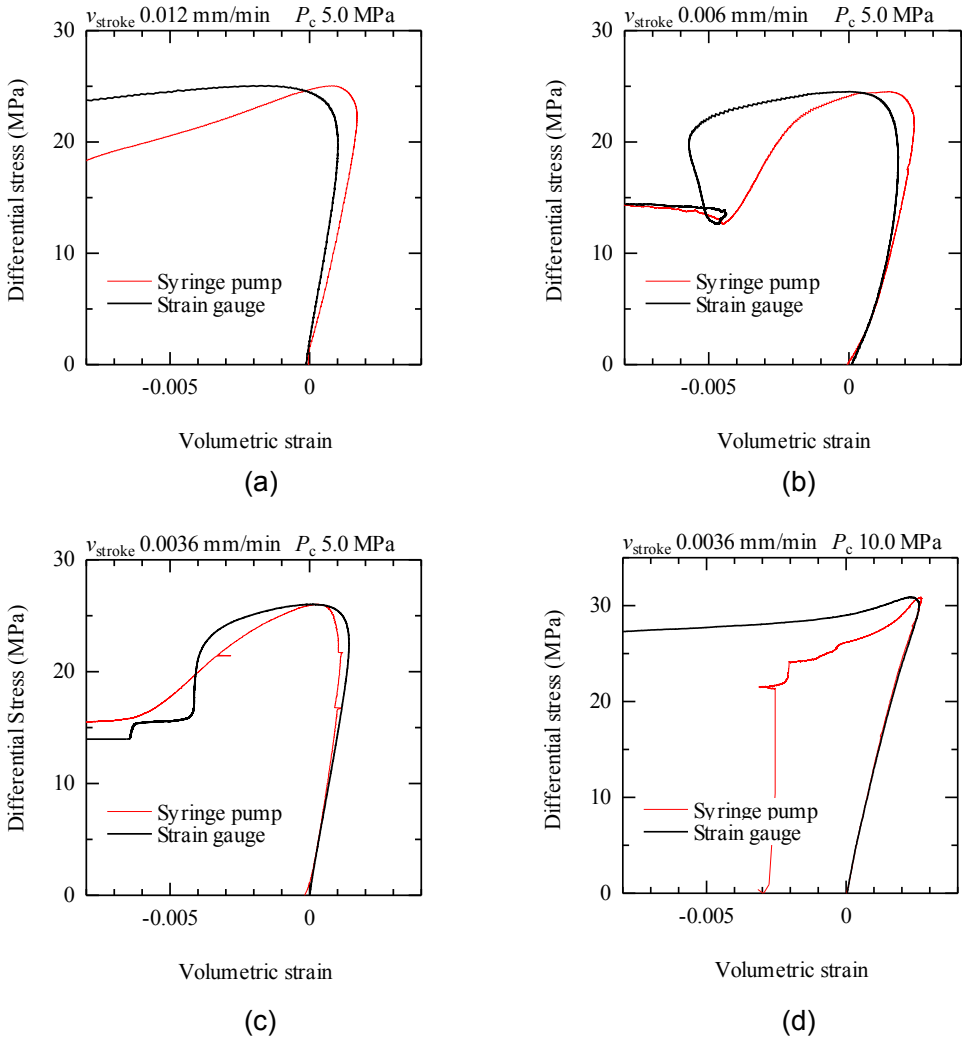

Figure 8. Volumetric strain measured by the syringe pump and strain gauges. v_{stroke} denotes displacing rate.

could induce decrease of mean axial stress and stiffness. **Figure 9** shows examples of partial rotational deformation. It involves rotation of a particle, opening of cracks parallel to the axial direction, growth of these cracks, sliding of wing cracks etc. This deformation could be linked to the increase in the permeability. In the region between peak strength and residual strength, the generation of macroscopic faults might have developed flow path. Deformation in residual strength region would be sliding of macroscopic fault. This sliding could be connected to crashing of asperities and closure of the fault planes.

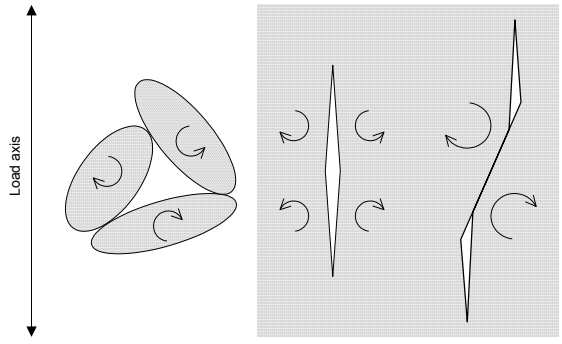

Figure 9. Illustration of partial rotational deformations.

4.2. Effect of confining pressure

Effect of confining pressure was noticeable in the results. The reason why change in permeability was small in the test under a confining pressure of 10.0 MPa would be because failure at high confining pressure was similar to plastic flow and fault planes did not open wide at failure. As the photograph in **Figure 6**, macroscopic faults were generated in all specimens but aperture of them is less apparent in case of the high confining pressure.

4.3. Difference of measured volumetric strain

Volumetric strain measured by syringe pump was close to that by strain gauges especially in case of a high confining pressure and a low displacing rate but not the same. This difference would be induced

by barreled deformation of specimen. Although end faces of the specimens were ground, some friction force should have occurred between a specimen and end pieces. This friction would have interrupted lateral expansion and affected on deformation and failure of specimens.

5. Conclusion

Permeability of Kimach sandstone in deformation and failure process under constant confining pressures was experimentally studied. The main results are as follows.

(1) In the low deviator stress region, the stress-strain relation was relatively linear and permeability decreased. Closure of flow path seems to induce permeability decrease.

(2) The stress-strain relation gradually became nonlinear and permeability increased as peak strength approached. Crack generation and growth would be the reason of the increase in permeability and nonlinear deformation.

(3) Deviator stress decreased and permeability increased in the period between peak strength and residual strength. Macroscopic rapture plane would be generated in this period.

(4) Permeability increased at first but gradually decreased with increased axial strain in the residual strength region. Closure of the fault planes would induce the decrease in permeability.

(5) The experiments were conducted under confining pressures of 5.0, 7.5 or 10.0 MPa. Permeability change was small under 10.0 MPa confining pressure and permeability varied more under 5.0 MPa confining pressure. This might be because failure under high confining pressure was similar to plastic flow and macroscopic rapture plane did not have large aperture.

(6) Volumetric strain was measured by strain gauges and the syringe pump. Results were almost the same. It is likely that deformation of the specimen pore was considerably larger than that of mineral particles.

Appendix: The approximate solution of the transient pulse method

The approximate solution of the transient-pulse method is derived as follows. Flow rate of upstream q_1 and downstream q_2 were assumed to be equal.

$$q_1 \cong q_2 = q\,. \tag{A1}$$

Water pressures of upstream p_1 and downstream p_2 were expressed as

$$p_1 = p_0 + \Delta p_0 - \frac{1}{S_1}\int_0^t q\mathrm{d}t\,, \tag{A2}$$

$$p_2 = p_0 + \frac{1}{S_2}\int_0^t q\mathrm{d}t\,, \tag{A3}$$

where p_0 is initial water pressure, Δp_0 is pulse increase of upstream water pressure, S_1 is compressive storage of upstream reservoir and S_2 is compressive storage of downstream reservoir.

Darcy's law yields

$$q = A\frac{k}{\mu L}\left(\Delta p - \frac{S_1+S_2}{S_1S_2}\int_0^t q\mathrm{d}t\right), \tag{A4}$$

where k is permeability coefficient, A is cross sectional area, μ is viscosity of water. Differentiating Eq. (6.4) with respect to time,

$$\frac{\mathrm{d}q}{\mathrm{d}t} = -A\frac{k}{\mu L}\frac{S_1+S_2}{S_1S_2}q\,. \tag{A5}$$

The solution of this eqation is

$$q = \exp\left(-A\frac{k}{\mu L}\frac{S_1+S_2}{S_1S_2}t\right). \tag{A6}$$

This is rewritten in terms of using fluid pressure.

$$\frac{\mathrm{d}\left[\ln\left(p_1-p_2\right)\right]}{\mathrm{d}t} = -A\frac{k}{\mu L}\frac{S_1+S_2}{S_1S_2}\,. \tag{A7}$$

This derivation is not the exactly same but almost similar to that of Brace et al. [3] (equations (2) and (3)). There are some cautions on utilizing of this solution. Water storage of reservoirs should be larger than water storage of a specimen, since water storage of a specimen is ignored in the derivation. Pulse pressure increase of upstream should be small since such water properties as density, viscosity and compressibility change as function of pressure.

References

[1] Ngwenya, B. T., Kwon, O., Elphick, S. C. and Main, I. G. (2003): Permeability Evolution During Progressive Development of Deformation Bands in Porous Sand Stones, Journal of Geophysical Research, Vol. 108, No. B7, pp. ECV6.1-ECV6.14, 2003.

[2] Kiyama, T. and Ishijima, Y. (2000, in Japanese): Permeability of Westerly granite around failure in Triaxial Compression Test, Proceeding of MMIJ Hokkaido Branch Annual Meeting (2000), pp. 39-40.

[3] Brace, W. F., Walsh J. B., and Frangos, W. T. (1968): Permeability of Granite under High Pressure, Journal of Geophysical Research, Vol. 73, NO. 6, pp. 2225-2236.

[4] Wyllie, M. R. J. and Gregory, A. R. (1955): Fluid Flow through Unconsolidated Porous Aggregates, Industrial & Engineering Chemistry, Vol. 47, No. 7, pp. 1379-1388.

[5] Kozeny, J. (1927) Uber Kapillare Leitung des Wasser im Boden, Sitzungsberichte der Akademie der Wissenschaften Wien, 136(2a), pp. 106–271.

[6] Carman, P. C. (1937): Fluid Flow through Granular Beds, Chemical Engineering Research and Design, Vol. 15a, pp. 150-166.

[7] Garrouch, A. A. Ali, L. and Qasem, F. (2001): Using diffusion and electrical measurements to assess tortuosity of porous media, Industrial & Engineering Chemistry Research., 40 (20), pp.

4363–4369.
[8] Hirono, T. Nakashima, S. Spiers, C. J. (2008): Measurements of Ionic Diffusivity in Various Rock Samples: Low Diffusivity Through Nanoscale Pores, International Journal of Rock Mechanics and Mining Sciences, Vol. 45, Issue 3, March 2008, p.p. 450-459.
[9] Takahashi, M. XuE, Z. and Koide, H. (1991, in Japanese) Permeability Characteristics of Inada Granite, Shirahama Sandstone, Kimachi Sandstone, and Neogene Argillaceous Rock, Geol. Surv. Japan, Vol. 42, No. 6/7, p.p. 305-331.
[10] Nakamura, D. Goto, T. Suzuki, T. Ito, Y. Yamashita, S. (2008, in Japanese): Basic Study on Frost Susceptibility of Rock -Understanding the Mechanism of Frost Heave Based on Comparison of the Internal Structure and the Physical Properties of Rock-, Journal of MMIJ, Vol. 124, No. 4, 5, p.p 231-239.
[11] Lin, W. Takahashi, M. (2000, in Japanese): Mercury Intrusion Porosimetry and Its Application for Determination of Pore Volume Distribution of Rock, Chishitsu News, No. 549, p.p. 61-68.
[12] Sugimoto, F., Matsuki, K., and Endo, O. (1985, in Japanese): On the Permeability of Rock Measured with Transient Pulse Method, Journal of the Japan Society of Engineering Geology, Vol. 26, No. 3, pp. 11-18.
[13] Kumakura, S. Kiyama, T. Nishimoto, S. Ishijima, Y. Fujii, Y. (2006, in Japanese): A Study on Permeability of Fractured Kimachi Sandstone, Procceding of MMIJ Hokkaido Branch Annual Meeting (2006), pp. 111-112.
[14] Fujii, Y. (2004, in Japanese): Ultra Compact Triaxial Cell for Triaxial Test of Rock, Proc. MMIJ Fall Meeting, (A)(B), pp. 73-74.
[15] Hsieh, P. A., Tracy, J. V., Neuzil, C. E., Bredehoeft, J. D., and Silliman, S. E., (1981): A Transient Laboratory Method for Determining the Hydraulic Properties of "Tight" Rocks - I. Theory, International Journal of Rock Mechanics and Mining Sciences & Geomechanics Abstracts, Vol. 18, pp. 245-252.